NATIONAL TRANSPORTATION SAFETY BOARD
Office of Research and Engineering
Materials Laboratory Division
Washington, D.C. 20594

December 6, 2014

MATERIALS LABORATORY FACTUAL REPORT Report No. 14-055

1. ACCIDENT

Place: Casselton, ND
Date: December 30, 2013
Vehicle: BNSF Grain Freight Car, G-RYLRGT9-26A
NTSB No.: DCA14MR004
Investigator: Richard Hipskind, RPH-10

2. COMPONENTS EXAMINED

Grain railcar wheelset (fractured at the axle)

3. GROUP MEMBERS

Erik Mueller, NTSB, RE-30
Michael Hiller, NTSB, RPH-10
Richard Hipskind, NTSB, RPH-10
Dennis Morgart, BNSF Railway Company
Byron Dickey, BNSF Railway Company
Huseyin Guzel, BNSF Railway Company
Steven Dedmon, Standard Steel

4. DETAILS OF THE EXAMINATION

On December 30, 2013, about 1411 central standard time, a westbound BNSF Railway (BNSF) grain train (G-RYLRGT9-26A) derailed 13 cars near Casselton, North Dakota. The grain train, operating on main track 1, consisted of two head-end locomotives, one rear distributed power locomotive, and 112 cars. One of the derailed cars, the 45th car from the head end, fouled main track 2. An eastbound BNSF petroleum crude oil unit train (U-FYNHAY4-05), operating on main track 2, collided with the derailed car that was fouling the track, causing the head-end locomotives and the first 21 cars of the train to derail. The petroleum crude oil unit train consisted of two head-end locomotives, one rear distributed power locomotive, and 106 cars.

A broken axle and two wheels were recovered at the accident site and were shipped to the NTSB Materials Laboratory for further evaluation and analysis. Figure 1 illustrates both sides of the fractured axle, as received. The axle fractured such that one segment was shorter than the other longer segment. The axle had fractured at an

internal void located along the axle radial centerline, approximately 15 inches from the wheelseat of the short axle segment. The mating fracture surfaces are shown in Figure 2 and Figure 3. The exposed void halves in the fracture surfaces were filled with debris consistent with post-derailment ground impact. This debris was removed during the examination.

The fracture surface of the long axle segment, located approximately 32 inches from the wheelseat, exhibited soot deposits and bluish heat tinting, consistent with exposure to fire. The inboard wheel plate also exhibited indications of fire exposure. Some rusting was observed in sporadic areas on the long axle shaft. The fracture surface exhibited a small outward lip on one side of the fracture surface.

The short axle segment was absent these indications of fire exposure. However, much of the fracture surface had been smeared and scraped consistent with post fracture batter.

4.1 Nondestructive Inspection and Group Exam Axle Sectioning

The axle fragments were inspected using ultrasonic testing (UT) by Level II and Level III certified operators from Testing Technologies, Inc.[1] The length of the axle body was examined (a radial inspection) after the surfaces had been cleaned and prepared in order to facilitate contact with the UT transducers using a couplant. The UT operators used a 1 inch transducer at 2.25 MHz frequency, with typical amplifications of 55 – 77 dB, depending on the feature being inspected. Both axle segments were inspected by radial UT, and the edge of the drop on the transducer were marked at the edges of the voids during this inspection.

The summary of the results is depicted on the axles in Figure 4. The open centerline void at the fracture surfaces was characterized as asymmetrical in shape based on the UT reflectance data. The larger axle segment contained two indications outboard of the exposed centerline void at the fracture surface. The UT personnel stated that the middle indication was approximately 3 inches long, located approximately midway between the fracture surface and wheel seat. The shorter axle segment contained one indication besides the centerline void at the fracture surface. This indication was approximately 1.5 inches, but only displayed approximately 10% loss of reflectance off the back wall. These indications were examined further, as discussed in Section 4.3.

The shorter axle segment was repositioned 90° to that shown in Figure 1 in order to facilitate an UT inspection from the free end (an axial inspection). This inspection configuration was similar to the UT inspection prescribed by applicable AAR M-101 specification at the time of the axle manufacture (1998 revision).[2] However, the inspection at manufacture differs, among other issues, in that the three outboard bore

[1] Testing Technologies, Inc. is a non-destructive testing service provider, located in Woodbridge, VA.
[2] The applicable specification for axle ultrasonic inspection, AAR M-101 (1998 revision), prescribed an axial end pulse-echo ultrasonic inspection using a 2.25 MHz frequency with quartz 1” square, quartz 1.125” round, or barium titanate 0.75 - 1.0” round transducers, at the discretion of the operator. Rejectable indications include those with amplitudes less than 40% full-screen height backwall reflection or greater.

holes present in the fracture axle are typically not yet machined before the UT inspection. The results from the axial UT inspection were deemed indeterminate by the inspecting personnel, who stated this was likely due to interference from the drilled cap screw holes (for securing the lock plate) and the rough texture and geometry of the back wall (the fracture surface).

After the UT inspections, the longer axle segment was repositioned to allow for sectioning. The axle segment was sectioned below the UT indication for the edge of the transducer drop (yellow line in Figure 4). The fracture surface was then sectioned approximately 1 inch below the lowest surface point. The axle cross-section below the fracture surface is depicted in Figure 5. A portion of the void, approximately 1.25 inches by 0.75 inches, was visible. This axle portion was then cross-sectioned through the void, as depicted by the yellow line in Figure 5. Figure 6 shows the sectioned void from both mating halves of the axle fragment. The void at this cross-section was approximately 1 to 1.25 inches deep.

The axle fracture surfaces were laser scanned using a FaroArm Quantum portable measurement probe and laser scanner. These data are compiled in Appendices A and B for the long axle segment and short axle segment fracture surfaces, respectively. The data for the sectioned void on the long axle segment, depicted in Figure 6, are compiled in Appendix C. Using the GeoMagic 12 rendering software on the FaroArm, the surface normals were inverted and merged to reconstruct the centerline void. This void reconstruction is compiled in Appendix D, the data from which was used for finite element modeling calculations.[3]

4.2 Axle Fracture Surface and Void Examination

The fracture surface of the longer axle segment is shown after sectioning in Figure 7. The fracture surface was cleaned using mild abrasion with Sparkleen soap solution, followed by ultrasonic cleaning in acetone. As labeled in Figure 8, approximately half of the fracture surface exhibited features consistent with progressive cracking. The morphology of the progressive region was consistent with cracks that initiated at the internal void and grew outward towards the axle surface. The ratchet marks on the fracture surface were consistent with multiple crack initiation sites and coalescence during crack propagation.

The remaining half of the fracture surface (from the long axle segment) exhibited an appearance consistent with overstress fracture. Figure 9 shows the edge of the progressive fracture, in contrast with the overstress regions. The progressive region appeared lighter in color and was generally flatter, oriented perpendicular to the axle length direction. Some faint crack arrest marks were visible in the progressive region. The overstress region exhibited rougher, tortuous surface texture. In addition, the heat tint coloring was more pronounced, with darker blues.

Much of the fracture surface had been battered, consistent with post-fracture damage from the derailment. Selected areas of the long axle segment fracture surface

[3] See *NTSB DCA14MR004 Vehicle Performance Study Report*

were relatively undamaged, such as depicted in Figure 10. This area, opposite the large progressive fracture region, contained small progressive cracks that had initiated at the centerline void. These small thumbnail-shaped cracks exhibited ratchet marks consistent with multiple crack initiation.

Examination in a scanning electron microscope (SEM) revealed fatigue striations present in the progressive fracture areas of the fracture surface (see Figure 12 and Figure 11). The striations emanated outward from the centerline void. No indications of features consistent with other fracture modes were found in the fatigue regions of the fracture surface.

The surface of the centerline void was examined in a SEM, as illustrated in Figure 13 and Figure 14. The surfaces of the void consisted of deep valleys protruding into the axle material, with rounded, smoothed peaks. Much of the surface of the void exhibited electron-charging effects in the SEM, consistent with non-conductive material (typically non-metallic). Figure 14 shows a closer view of the void surface, exhibiting blocky non-metallic phases. Inspection of these phases using energy dispersive x-ray spectroscopy (EDS) revealed aluminum and silicon oxides. The other script-shaped surface features exhibited compositions consistent with the remainder of the void surface.

4.3 Examination of Additional Internal Indications

On July 28, 2014, the remainder of the axle was sectioned at Standard Steel, LLC in Burnham, PA. The axle fragments had been removed from the wheels, were inspected using a longitudinal ultrasonic inspection, and were sectioned longitudinally along the centerline to determine if other void indications were present inside the axle. Ultrasonic inspection performed at Standard Steel found one indication on the short axle fragment.

Figure 15 and Figure 16 show the voids observed after cross sectioning the axle fragments. The short axle fragment contained three voids, and the long axle fragment exhibited two voids—these voids were observable to the unaided eye. The second void from the wheel seat journal on the short axle segment (Figure 15) was consistent with the location of the observed indication from the ultrasonic inspection.

All of these voids are shown magnified in Figure 17, ordered from the near the outboard wheel seat journal on the short axle segment (left in Figure 15) to near the wheel seat journal outboard on the long axle segment. All of these voids were generally flattened, oriented along the forging (longitudinal) direction. All of the voids were considerably smaller in volume than the large centerline void at the fracture surface—the largest void was approximately 0.2 inches in the longest direction, located along the centerline location of the axle.

One of the voids (shown in Figure 17c), was sectioned, mounted, polished and etched using 2% Nital solution. This void is shown in Figure 18, with the etchant having revealed the grain flow about the expose voids. No overt changes to the microstructure were observed adjacent to the voids (see Figure 19). Figure 20 shows a closer view of

the axle microstructure. The microstructure consisted of a fine pearlite structure, with proeutectoid ferrite dispersed between the pearlite colonies. This microstructure morphology was consistent throughout all the areas inspected.

The cross-sectioned void was inspected using the SEM. Smaller areas of non-metallic material were observed along the periphery of the void surface. One such area is illustrated in Figure 21. This material was inspected using EDS, and its chemical composition was found to be consistent with aluminum oxide.

4.4 Axle Material Properties

The journal from the shorter axle fragment was sectioned and sent to Lehigh Testing Laboratories, Inc. for mechanical and chemical testing.[4] Six specimens were machined from the outer areas of the journal. Each specimen was tensile tested and chemically inspected to determine the material composition. The average chemical composition is shown in Table 1. All specimens were consistent with the prescribed composition from AAR M-101-90 (1998 Rev). All the specimens exhibited compositions consistent with UNS G10500, G10530, and G10550; one of the specimens was also consistent with UNS G10490.

The mechanical properties of all the tensile specimens met the tensile requirements of AAR M-101-90, Grade F (1998 Rev). The average mechanical properties are listed in Table 2. Full details of the testing results are shown in Appendix E.

4.5 Wheels and Axle Bearings

The wheels affixed to the fractured axle were inspected as part of the examination. Figure 22 focuses on the wheel attached to the short axle segment (S/N 23693), as received. The markings on the gage side (facing inboard) of the short axle segment wheel are shown in Figure 23. The markings were:

01 10 SW C H36 23693

This wheel exhibited randomly oriented scratches, streaks, and gouges on the faces of both sides of the wheel. However, there were no indications of gross deformation or warping on the wheel. These witness marks were consistent with damage incurred during the derailment after the axle fractured. The rail contact surfaces of the wheel were intact, with no indications of wear, spalling, cracking, or denting. No indications of damage to the wheel flange were observed.

A portion of the axle bearing outboard of the wheel had fractured (see Figure 24). However, the shapes of the fracture, as well as features on the fracture surface, were consistent with overstress fracture consistent with damaged incurred during the derailment. Some fretting was observed around the axle journal seat adjacent the wheel

[4] Lehigh Testing Laboratories, Inc. is a materials testing, inspection, and failure analysis laboratory located in New Castle, DE.

(see Figure 25). However, there was no indication that this wear was related to the axle fracture.

Figure 26 depicts the wheel affixed to the long axle segment (S/N 23730), after cleaning to remove material consistent with burned material, such as grain, lost during the derailment. The marking on the inside face of the wheel, displayed in Figure 27, were:

01 10 SW C H36 23730

This wheel's surfaces exhibited darkening on one side, consistent with exposure to fire. No gross deformation was observed in these areas, indicative that the fire exposure was not long-term. The opposite side exhibited uniform surface rust. This rust was consistent with exposure to water after the derailment.

The flange and rail contact surfaces on one side of the wheel exhibited gouging and impact marks consistent with damage incurred after derailment. No indications of other damage on the wheels were observed. Some chatter marks were observed on the long axle segment adjacent to the inboard side of the wheel seat, but no indications of fretting were observed consistent with the short axle segment (see Figure 28).

Erik Mueller
Materials Research Engineer

Table 1 – Average chemical composition (in wt. %) of the short axle fragment journal, compared with requirements for AAR M101-90 Grade F (1998 rev), UNS G10500, UNS10530, UNS G10550, and UNS G10490.

Standard	C	Mn	Si	P	S	Cu	Ti	Cr	N
Axle Avg.	0.54	0.79	0.29	0.016	0.032	0.27	0.022	0.12	0.10
AAR M101	0.45-0.59	0.60-0.90	>0.15	<0.045	<0.050				
UNS G10500	0.48-0.55	0.60-0.90		<0.040	<0.050				
UNS G10530	0.48-0.55	0.70-1.00		<0.040	<0.050				
UNS G10550	0.50-0.60	0.60-0.90		<0.040	<0.050				
UNS G10490	0.46-0.53	0.60-0.90		<0.040	<0.050				

Table 2 – Average mechanical properties from tensile testing of the short axle fragment journal, compared with the minimum requirements for AAR M101-90 Grade F (1998 rev).

Standard	Upper Yield Point (ksi)	Lower Yield Point (ksi)	Ultimate Tensile Strength (ksi)	Yield Point Elongation (%)	Elongation in 2 in. (%)	Reduction in Area (%)
Axle Avg.	55.6	52.6	99.7	9.0	25	48
AAR M101		50	88		22	37

Figure 1 – The long and short segments of the fractured axle, as received.

Figure 2 – The fracture surface of the short axle segment, as received.

Figure 3 – The fracture surface of the long axle segment, as received.

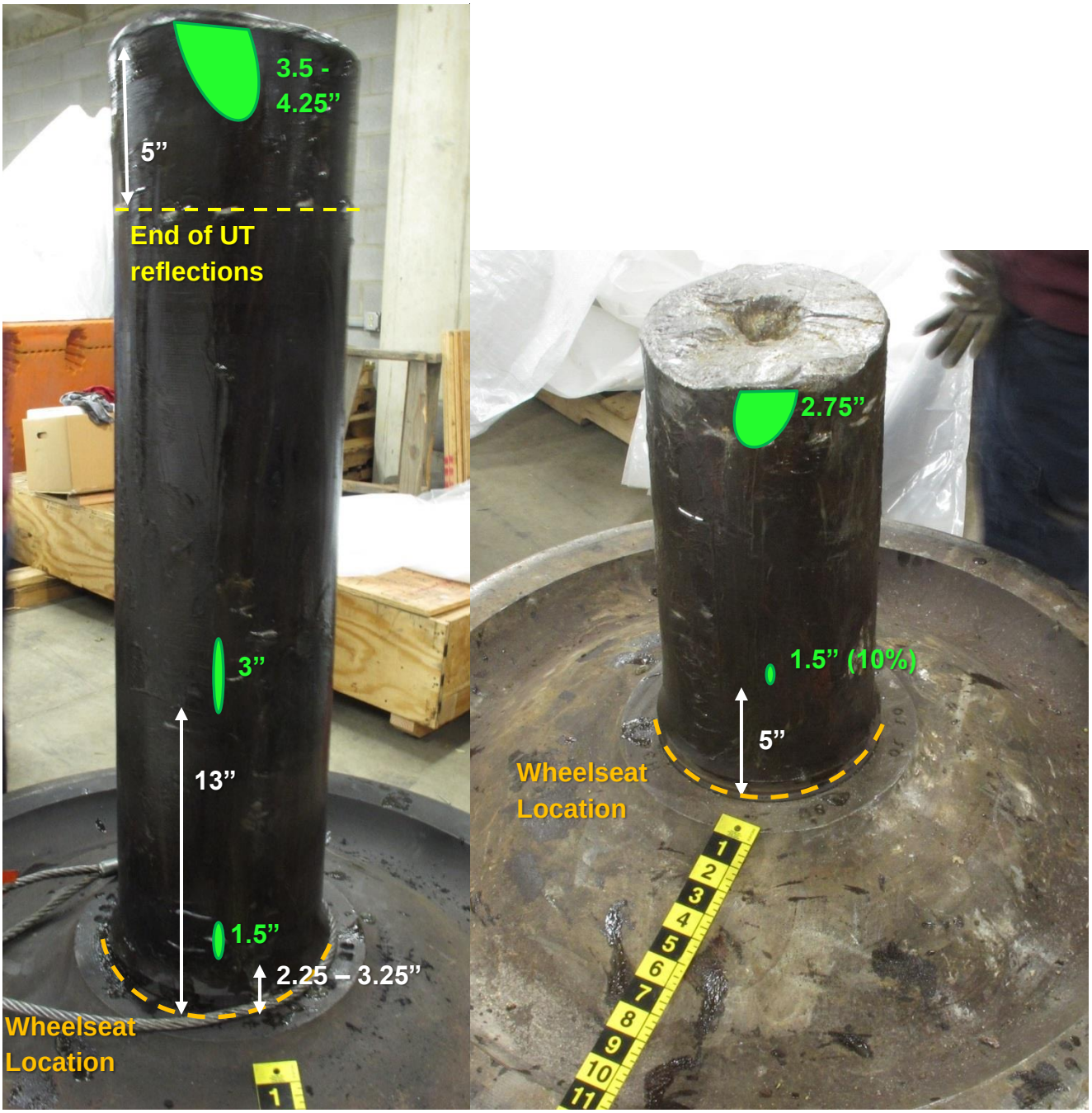

Figure 4 – The axle segments after UT NDT, with the green marks showing the relative locations and distances of the indications, based on the edge of the drop in UT transducer reflectance. The distances are relative to the wheel seat on the axle (dashed orange lines), or fracture surface.

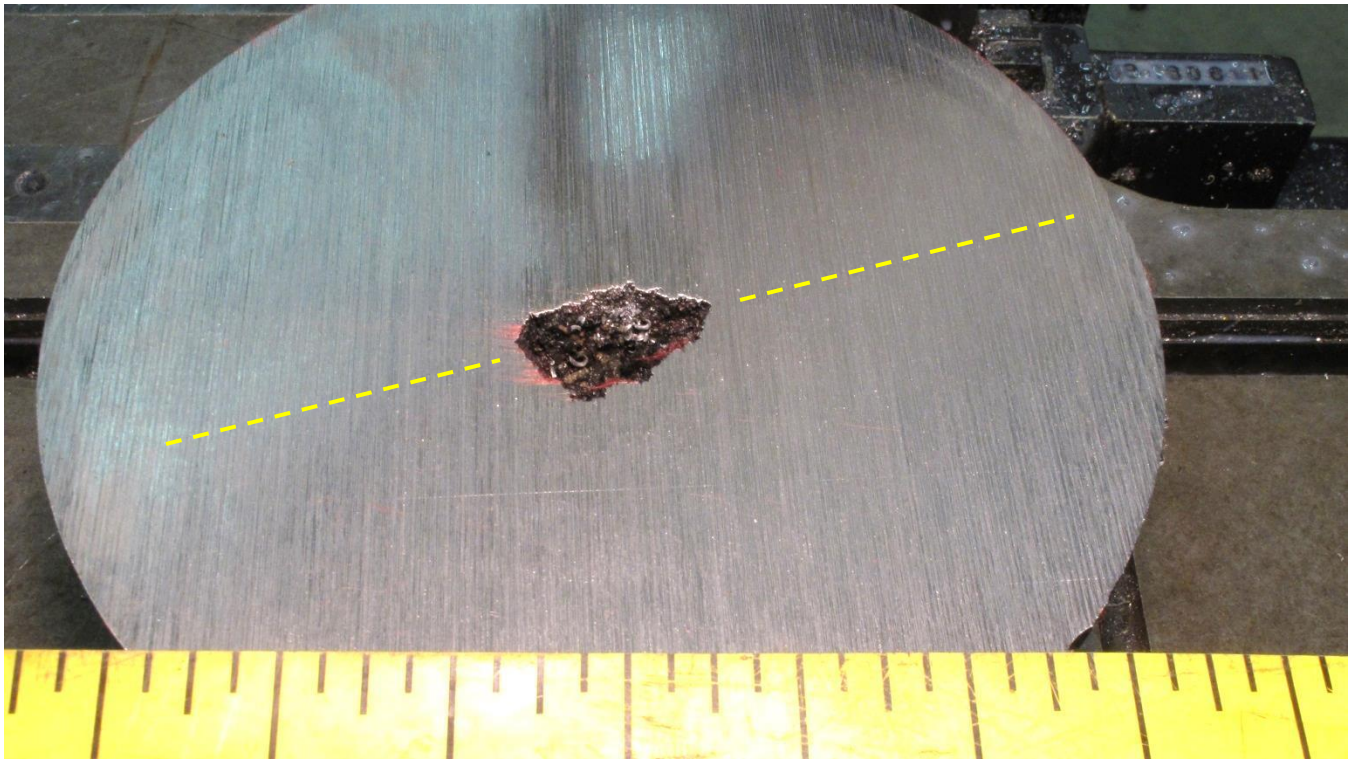

Figure 5 – The internal centerline void on the longer axle segment, after removal of the fracture surface (approximately 1 inch depth). The void measured 1.25” x 0.75”. The dashed line represents the cross-section shown in Figure 6.

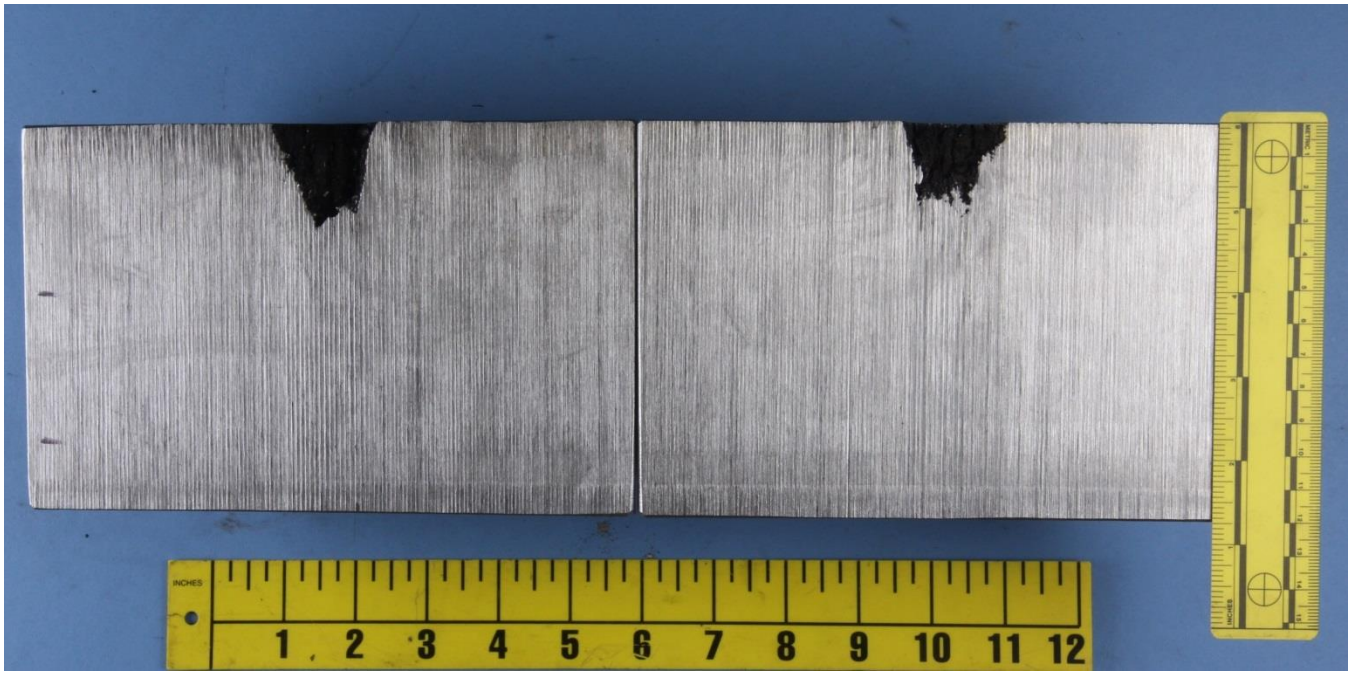

Figure 6 – The internal void from Figure 5 after sectioning down the middle.

Figure 7 – The longer axle segment fracture surface, after removal.

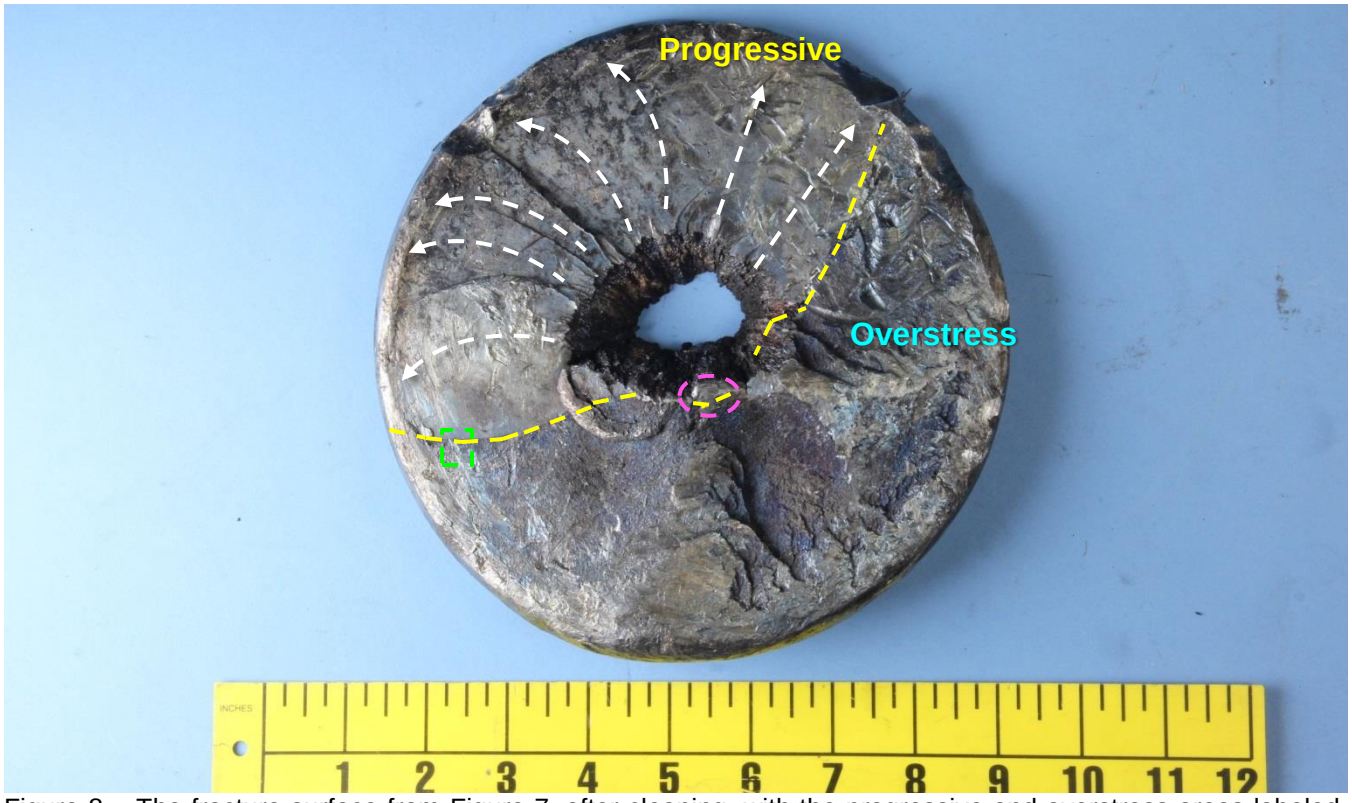

Figure 8 – The fracture surface from Figure 7, after cleaning, with the progressive and overstress areas labeled. The dashed line is the boundary between the progressive and overstress regions. The green dashed box is magnified in Figure 9, and the dashed oval is magnified in Figure 10.

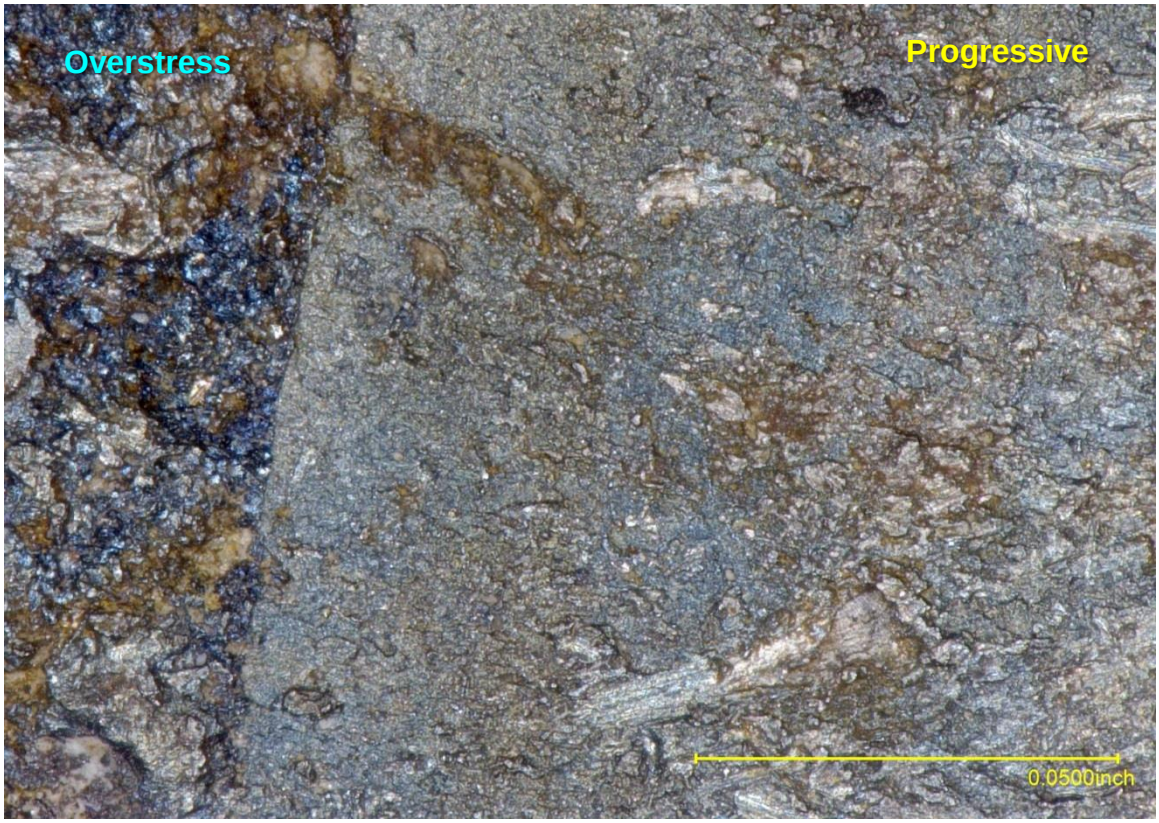

Figure 9 – Edge of the progressive crack on the axle fracture surface.

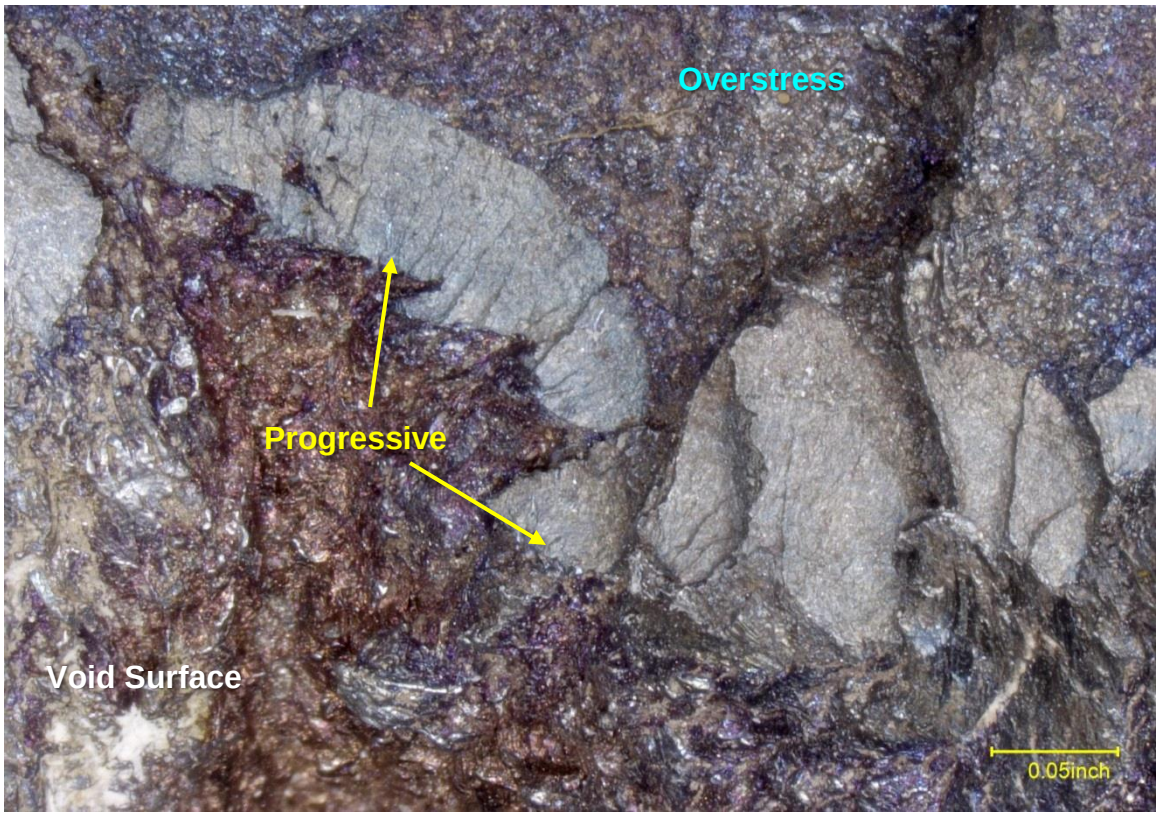

Figure 10 – Small fatigue cracks that had initiated and grew from the internal void in the axle.

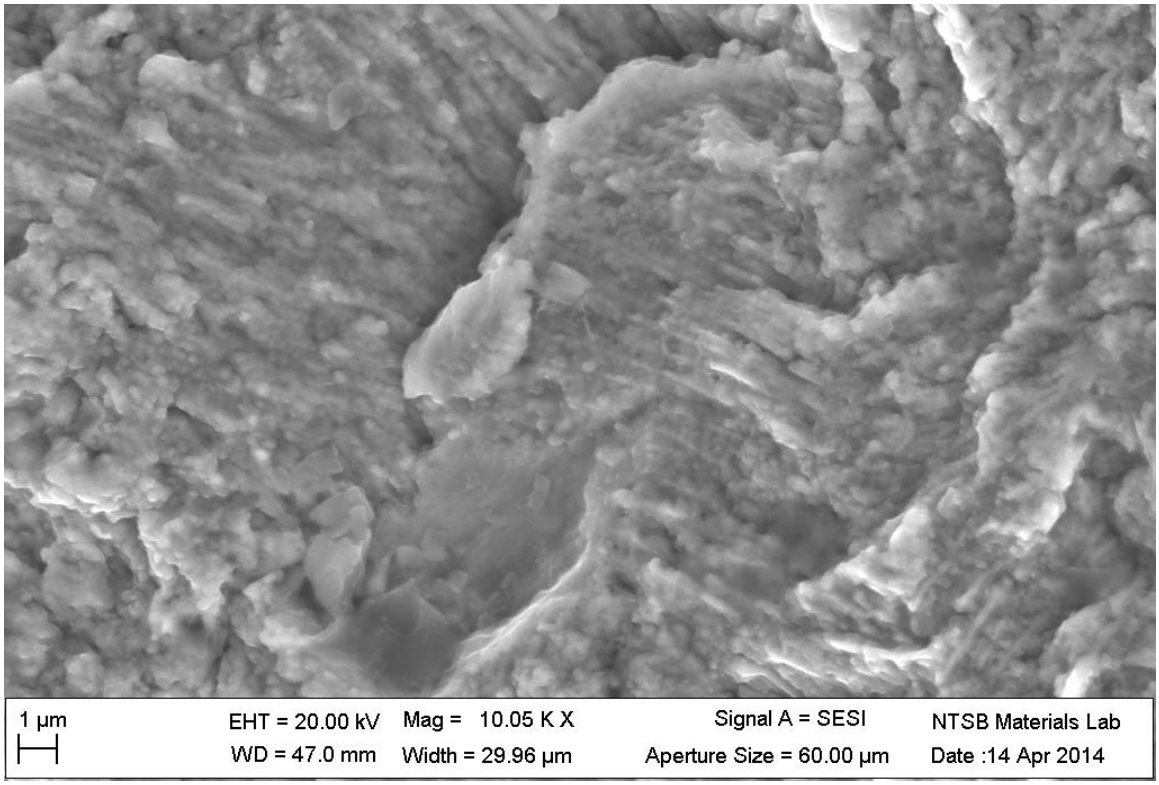

Figure 11 – SE micrograph of oxidized fatigue striations on the long axle fracture surface.

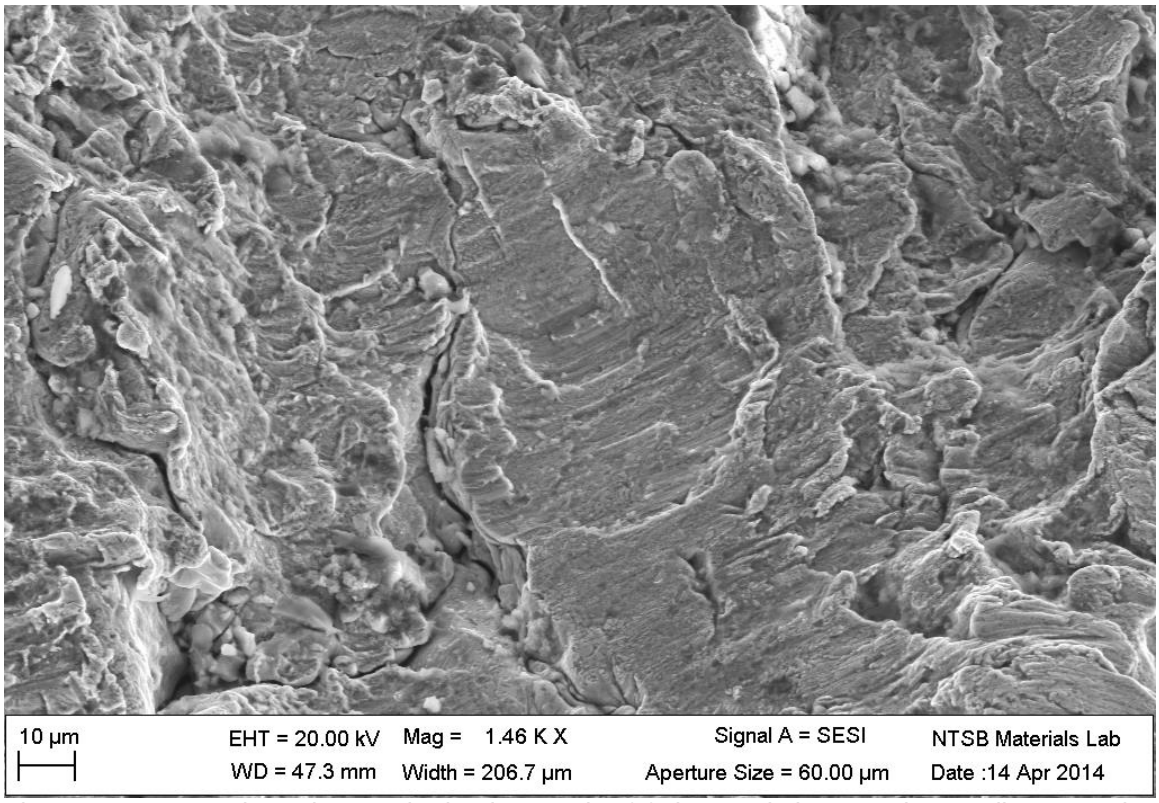

Figure 12 – Secondary electron (SE) micrograph of fatigue striations on the small progressive cracks adjacent to the void, depicted in Figure 10.

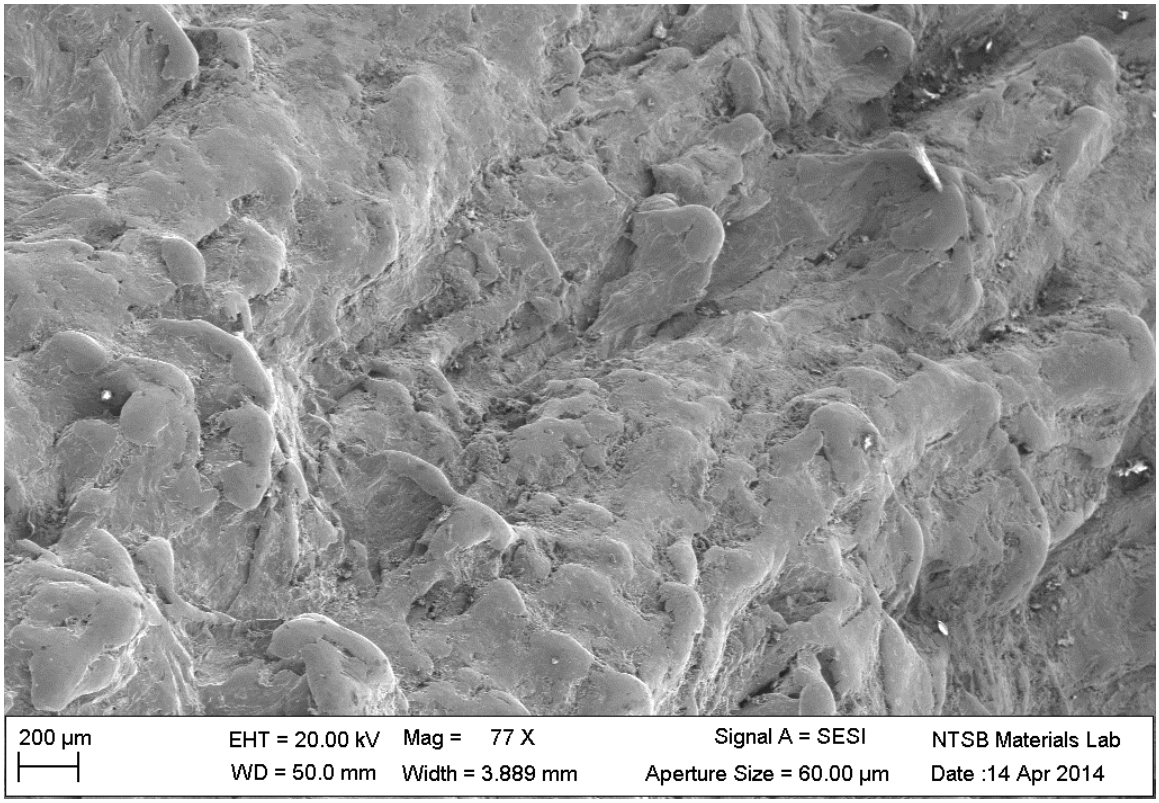

Figure 13 – SE micrograph of the internal void surface, showing rounded, rippled edges.

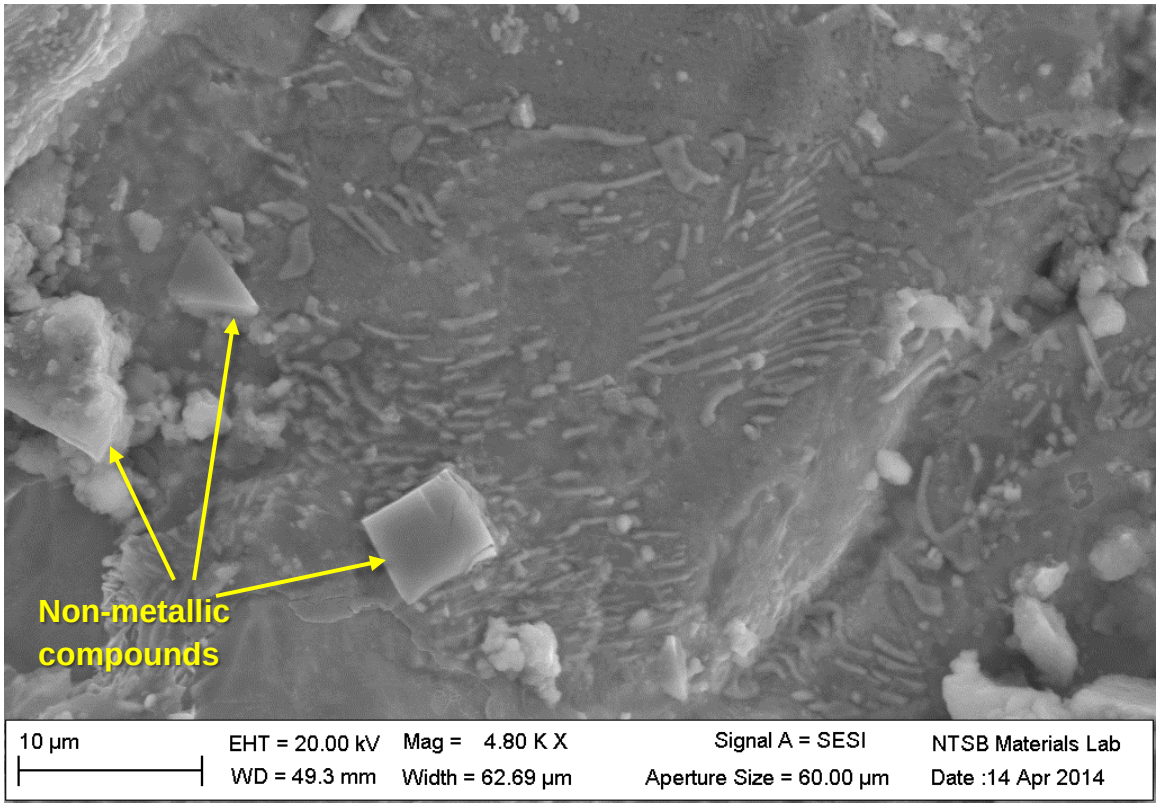

Figure 14 – SE micrograph of a closer view of the internal void surface.

Figure 15 – Cross section of the short side axle fragment, showing three small voids along the centerline.

Figure 16 – Cross section of the long side axle fragment, showing two small voids along the centerline.

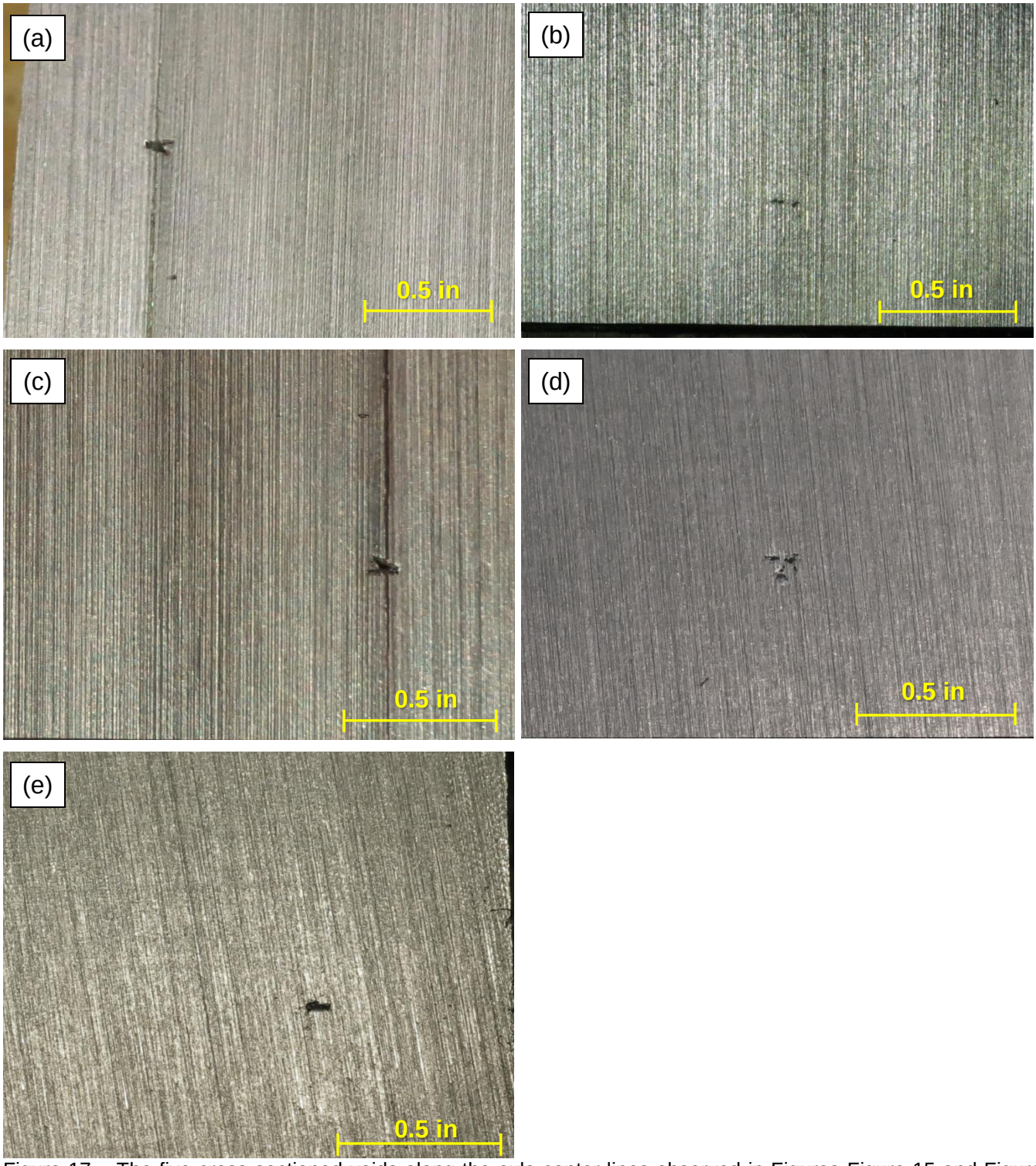

Figure 17 – The five cross-sectioned voids along the axle center lines observed in Figures Figure 15 and Figure 16.

Figure 18 – Optical metallograph of a cross-section through a small void in the centerline of the axle (etched with 2% Nital). The boxed area is shown in Figure 19.

Figure 19 – Optical metallograph showing the microstructure of the axle, showing a small void, the boxed area in Figure 18 (etched with 2% Nital).

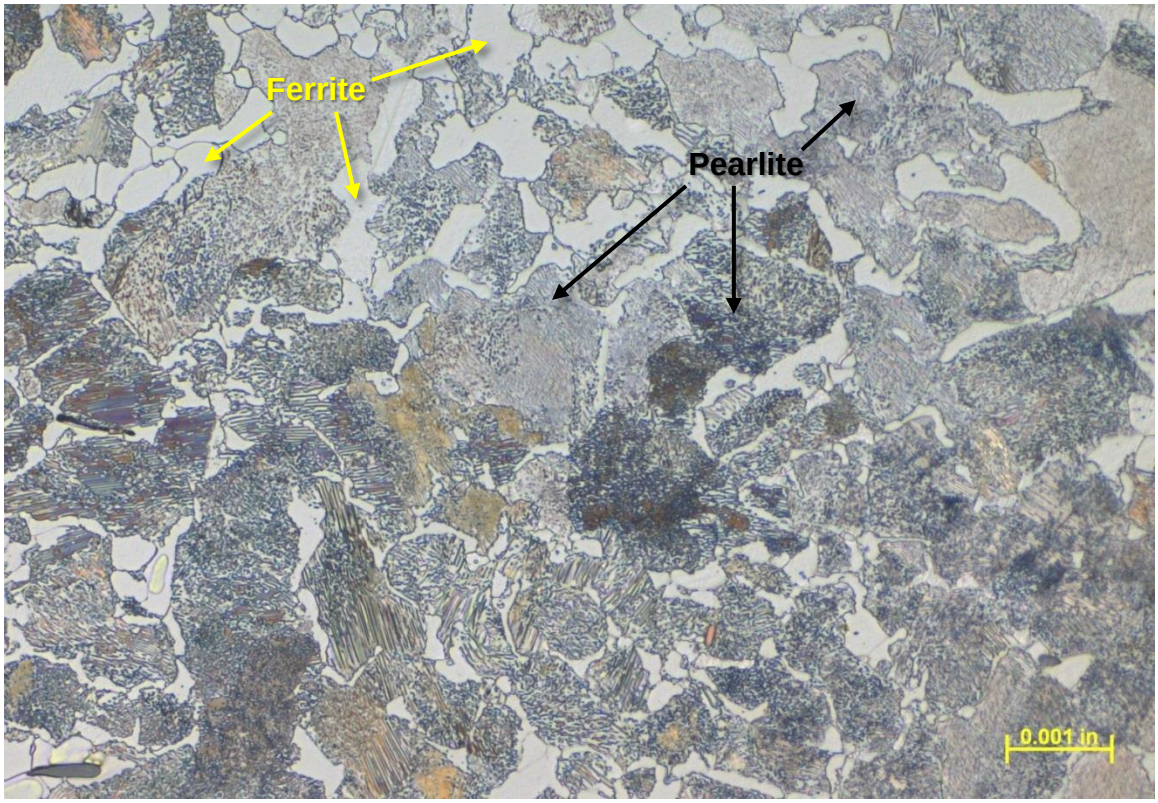

Figure 20 – Optical metallograph showing the microstructure of the axle, with colored pearlite between colorless ferrite (etched with 2% Nital).

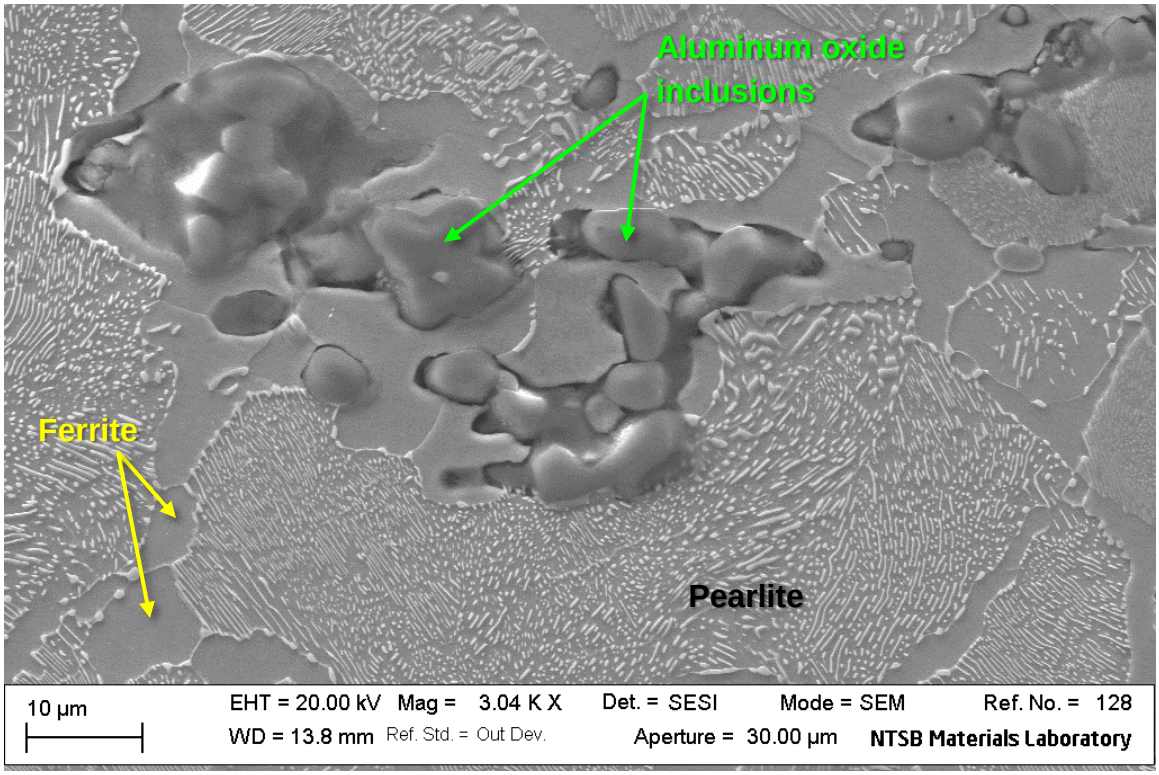

Figure 21 – SE micrograph of small inclusions near the void in Figure 19. These inclusions were consistent with aluminum oxide.

Figure 22 – The wheel on the short side of the axle, as received.


Figure 23 – Markings on the inside face of the short axle wheel.

Figure 24 – Axle bearing from the short axle segment.

Figure 25 – Possible fretting around the wheel seat of the short axle segment.

Figure 26 – The wheel from the long axle segment, after cleaning.

Figure 27 – Markings on the inside face of the wheel attached to the long axle segment.

Figure 28 – Chatter marks on the body and in-board wheel seat of the long axle.

A. APPENDIX A – 3-DIMENSIONAL LASER SCAN OF LONG AXLE SEGMENT FRACTURE SURFACE

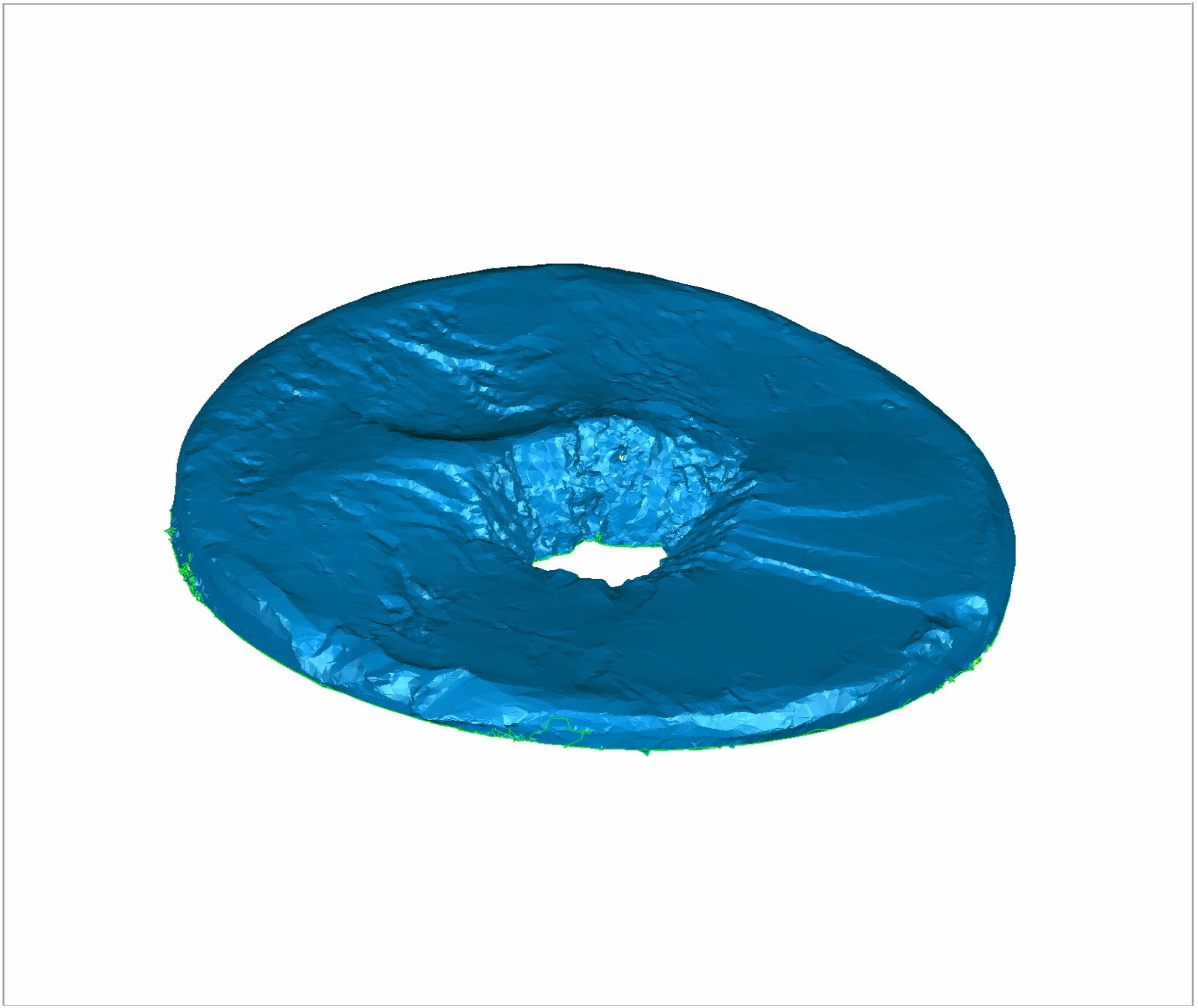

Click on the image to activate the 3D Model.

B. APPENDIX B – 3-DIMENSIONAL LASER SCAN OF THE SHORT AXLE SEGMENT FRACTURE SURFACE

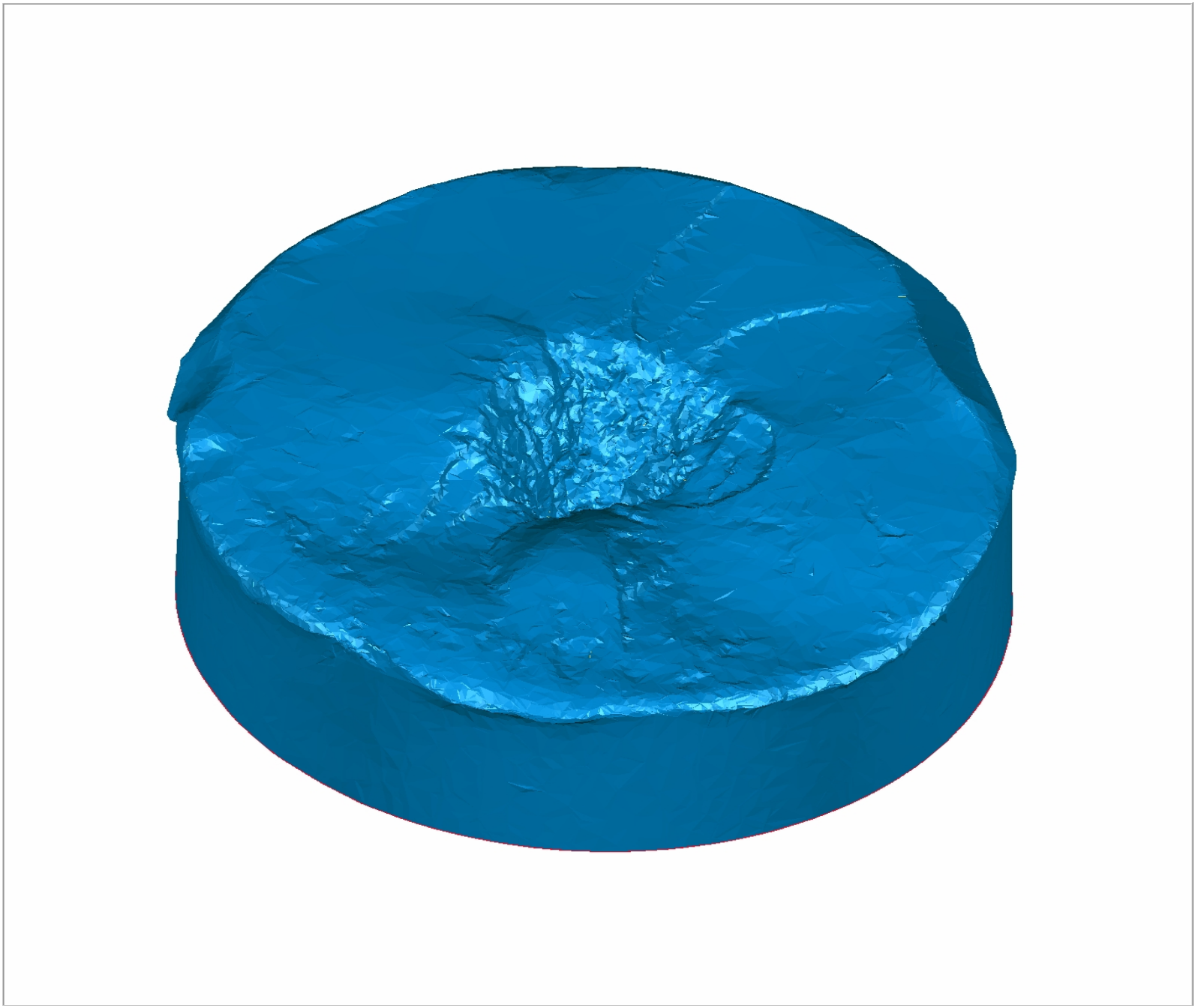

Click on the image to activate the 3D Model.

C. APPENDIX C – 3-DIMENSIONAL LASER SCAN OF THE INTERNAL VOID BELOW THE FRACTURE SURFACE OF THE LONG AXLE SEGMENT

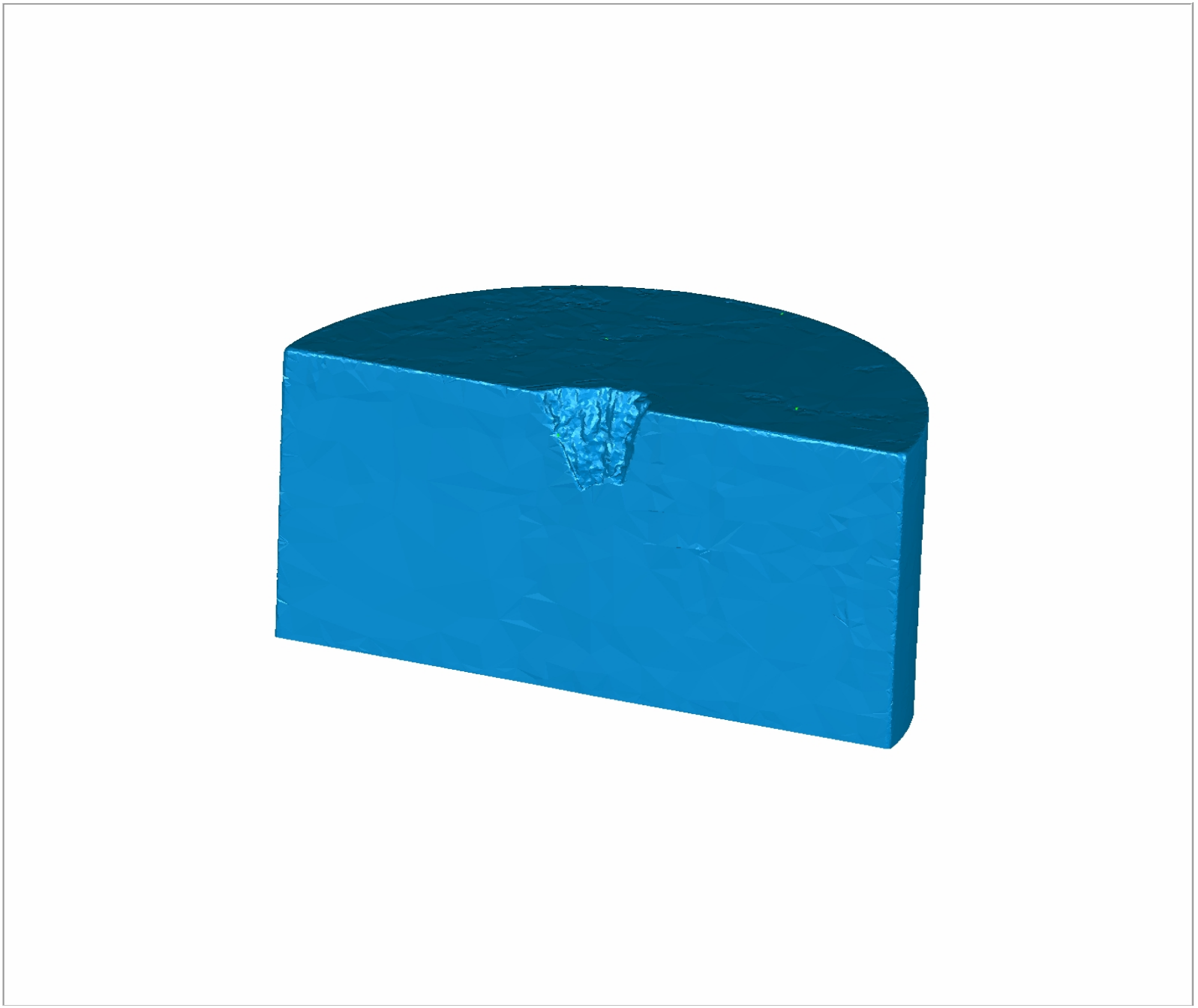

Click on the image to activate the 3D Model.

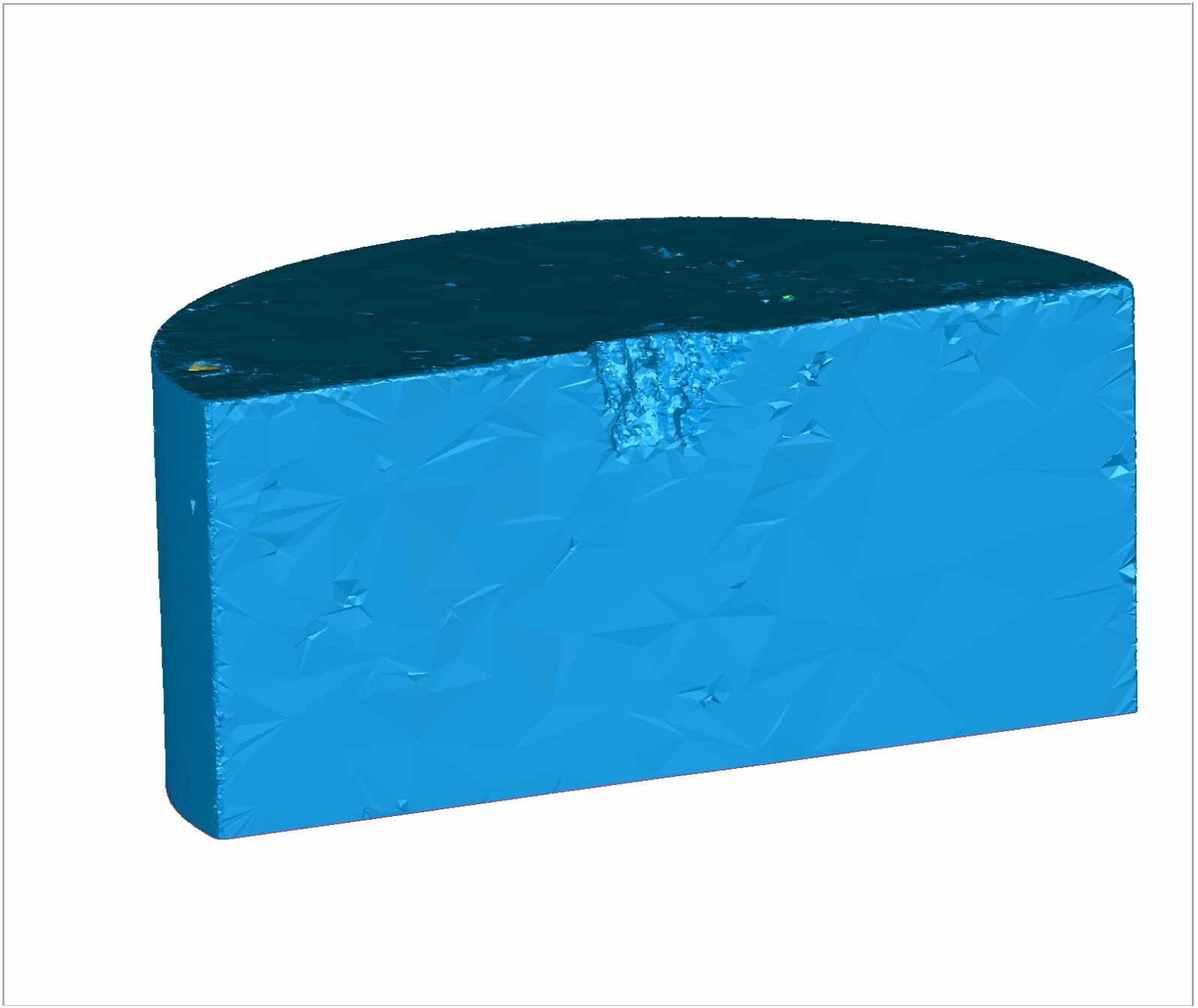

Click on the image to activate the 3D Model.

D. APPENDIX D – 3-DIMENSIONAL REPRESENTATION OF THE INTERNAL VOID SURFACES

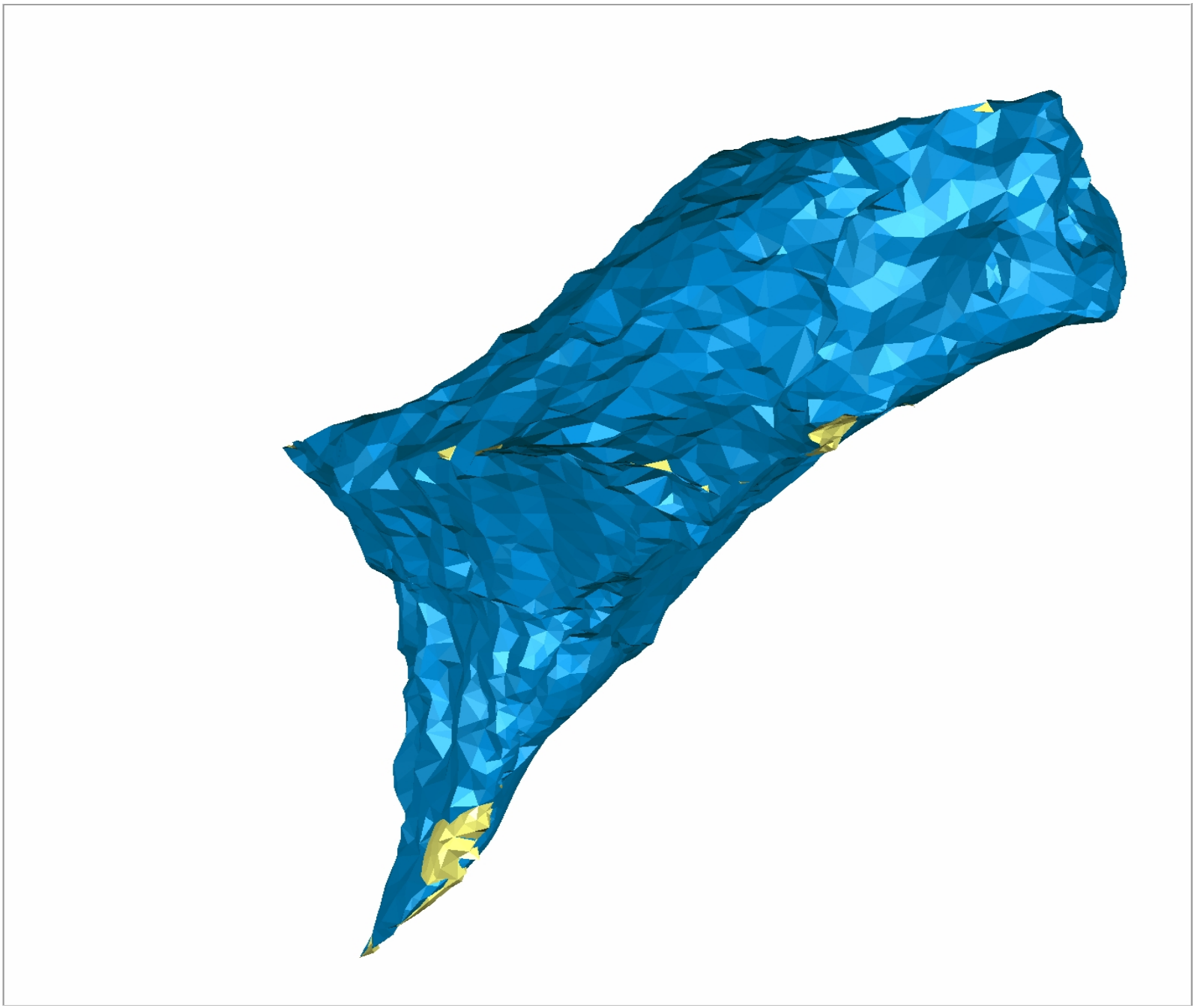

Click on the image to activate the 3D Model.

E. APPENDIX E – MECHANICAL AND CHEMICAL COMPOSITION TESTING RESULTS FROM LEHIGH TESTING INC.

Lehigh Testing Laboratories, Inc.
A Subsidiary of THE MMR GROUP, INC.
308 WEST BASIN ROAD • P.O. BOX 903 • NEW CASTLE, DE 19720
(302) 328-0500 • FAX (302) 328-0417

THE MMR GROUP, INC. an ESOP Company

TEST REPORT

NATIONAL TRANSPORTATION SAFETY BOARD
ATTENTION: ERIK MUELLER
490 L'ENFANT PLAZA EAST
WASHINGTON, DC 20594

DATE: August 22, 2014
PO NO: **VERBAL**
LEHIGH NO: **R-29-10**
PAGE: 1 of 1

MATERIAL: CARBON STEEL
SAMPLE DESIGNATION: (1) SAMPLE LOT: NTSB #DCA14MR004, FREIGHT AXLE

CHEMICAL ANALYSIS (%)

	1	2	3	4	5	6
Carbon	0.52	0.54	0.54	0.54	0.54	0.54
Sulfur	0.032	0.031	0.032	0.032	0.033	0.032
Manganese	0.80	0.77	0.79	0.78	0.80	0.80
Phosphorus	0.018	0.013	0.017	0.015	0.016	0.016
Silicon	0.30	0.29	0.30	0.29	0.29	0.29
Nickel	0.07	0.07	0.07	0.07	0.07	0.07
Chromium	0.12	0.12	0.12	0.12	0.12	0.12
Copper	0.27	0.27	0.27	0.27	0.27	0.26
Titanium	0.03	0.02	0.02	0.02	0.02	0.02
Vanadium	0.009	0.008	0.009	0.008	0.009	0.007
Cobalt	0.007	0.007	0.007	0.007	0.007	0.007
Niobium	0.003	<0.001	<0.001	<0.001	<0.001	<0.001
Tin	0.02	0.02	0.02	0.02	0.02	0.02
Tungsten	0.009	0.005	0.006	0.004	0.006	0.004
Lead	0.004	0.004	0.004	0.003	0.004	0.002
Aluminum	0.009	<0.004	0.005	<0.004	0.006	<0.004
Arsenic	0.010	0.006	0.006	0.006	0.008	0.003
Molybdenum	0.02	0.02	0.02	0.02	0.02	0.02
Nitrogen	0.011	0.010	0.010	0.010	0.010	0.010

Material (Samples 1 - 6) meets the chemical composition of UNS G10500, G10530 & G10550 with the exception of Sample #1 which also meets UNS G10490.

Procedure: *QA-CH-P-048 Rev 1 (Leco C&S), QA-CH-P-124 Rev 1 (ICP), QA-CH-P-122 Rev 1 (Leco N)*

Lehigh Testing Laboratories, Inc.

Deborah A. Hotra

Deborah A. Hotra, Senior Lab. Technician

Lehigh Testing Laboratories, Inc.
A Subsidiary of THE MMR GROUP, INC.
308 WEST BASIN ROAD • P.O. BOX 903 • NEW CASTLE, DE 19720
(302) 328-0500 • FAX (302) 328-0417

THE MMR GROUP, INC. an ESOP Company

TEST REPORT

NATIONAL TRANSPORTATION SAFETY BOARD
ATTENTION: ERIK MUELLER
490 L'ENFANT PLAZA EAST
WASHINGTON, DC 20594

DATE: August 22, 2014
PO NO: **VERBAL**
LEHIGH NO: **R-29-10**
PAGE: 1 of 1

MATERIAL: CARBON STEEL DOUBLED NORMALIZED AND TEMPERED
SPECIFICATION: AAR M-101-90 GRADE F
SAMPLE DESIGNATION: (1) SAMPLE LOT: NTSB #DCA14MR004, FREIGHT AXLE

MECHANICAL PROPERTIES (Per ASTM A370-12a)
LONGITUDINAL TENSILES

	1	2	3	4	5	6
Diameter (inches):	0.500	0.496	0.498	0.496	0.492	0.494
Area (square inches):	0.1963	0.1932	0.1948	0.1932	0.1901	0.1917
Upper Yield Point (psi):	58,100	55,700	57,900	56,100	52,600	53,300
Lower Yield Point (psi):	54,600	53,300	54,400	53,300	49,700	50,200
Yield Point Elongation %:	9.5	8.8	9.5	8.6	8.4	9.0
Ultimate Tensile Strength (psi):	102,500	102,300	102,800	97,400	96,400	96,900
Elongation (%) in 2":	24	26	24	25	25	26
Reduction of Area (%):	48	48	45	51	49	49

Based on the above testing this material meets the tensile requirements of AAR M-101-90 GRADE F.

Lehigh Testing Laboratories, Inc.

Kenneth M. Petito

Kenneth M. Petito, Supvr., Mechanical Testing

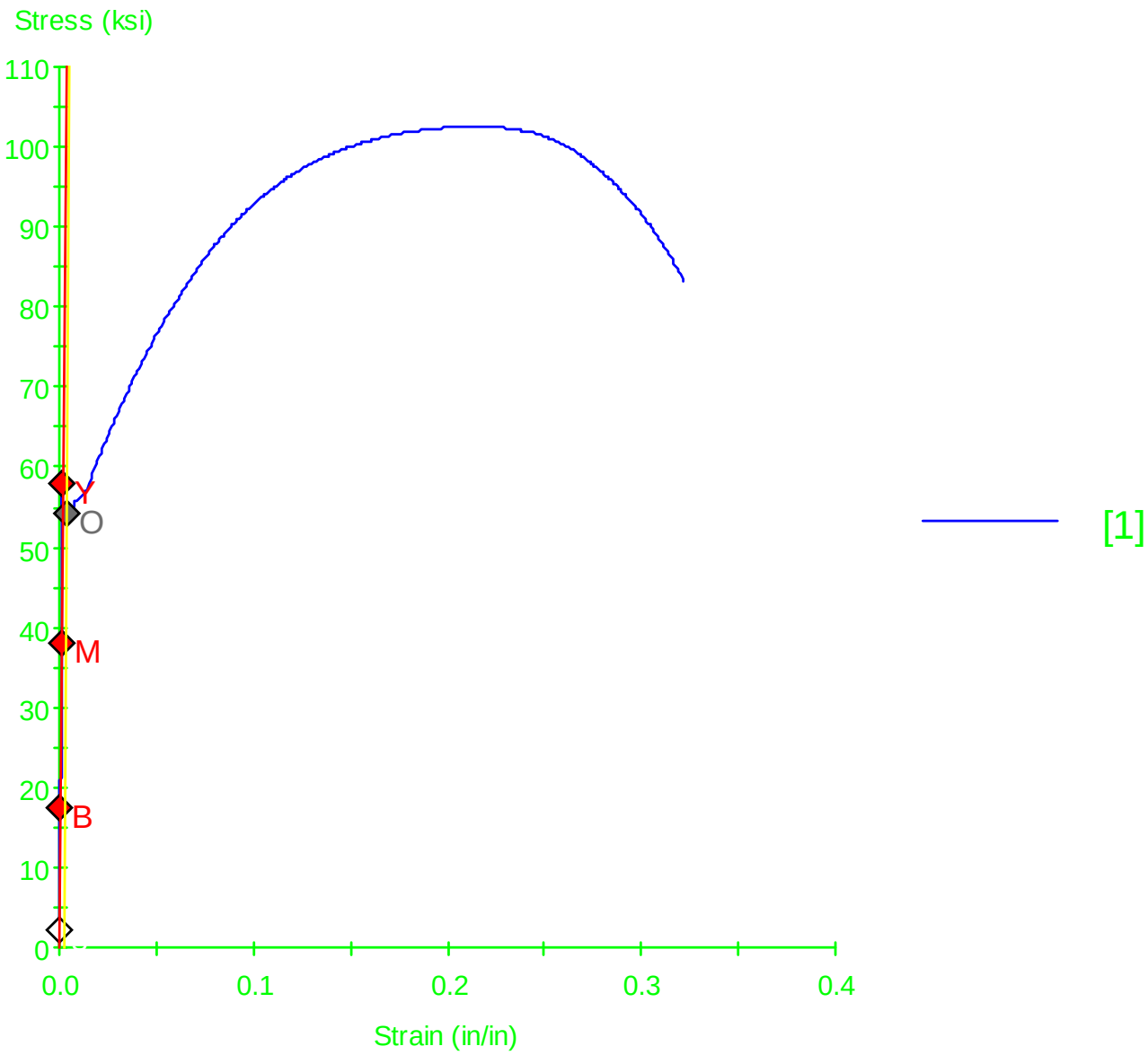
Stress (ksi)
110
100
90
80
70
60
50
40
30
20
10
0
Y
O
M
B
0.0
0.1
0.2
0.3
0.4
Strain (in/in)
[1]

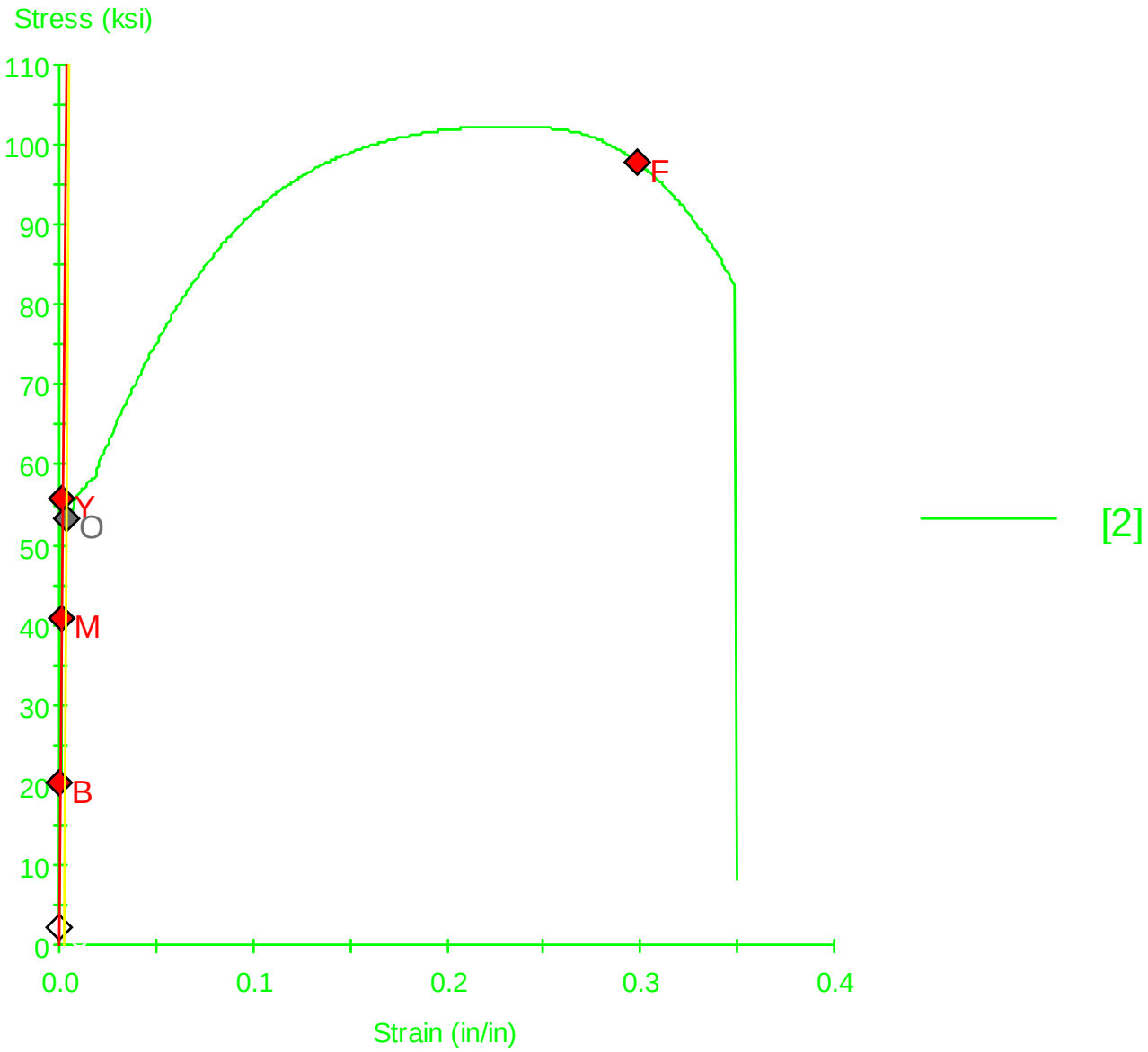
Stress (ksi)
110
100
90
80
70
60
50
40
30
20
10
0
F
Y
O
M
B
0.0
0.1
0.2
0.3
0.4
Strain (in/in)
[2]

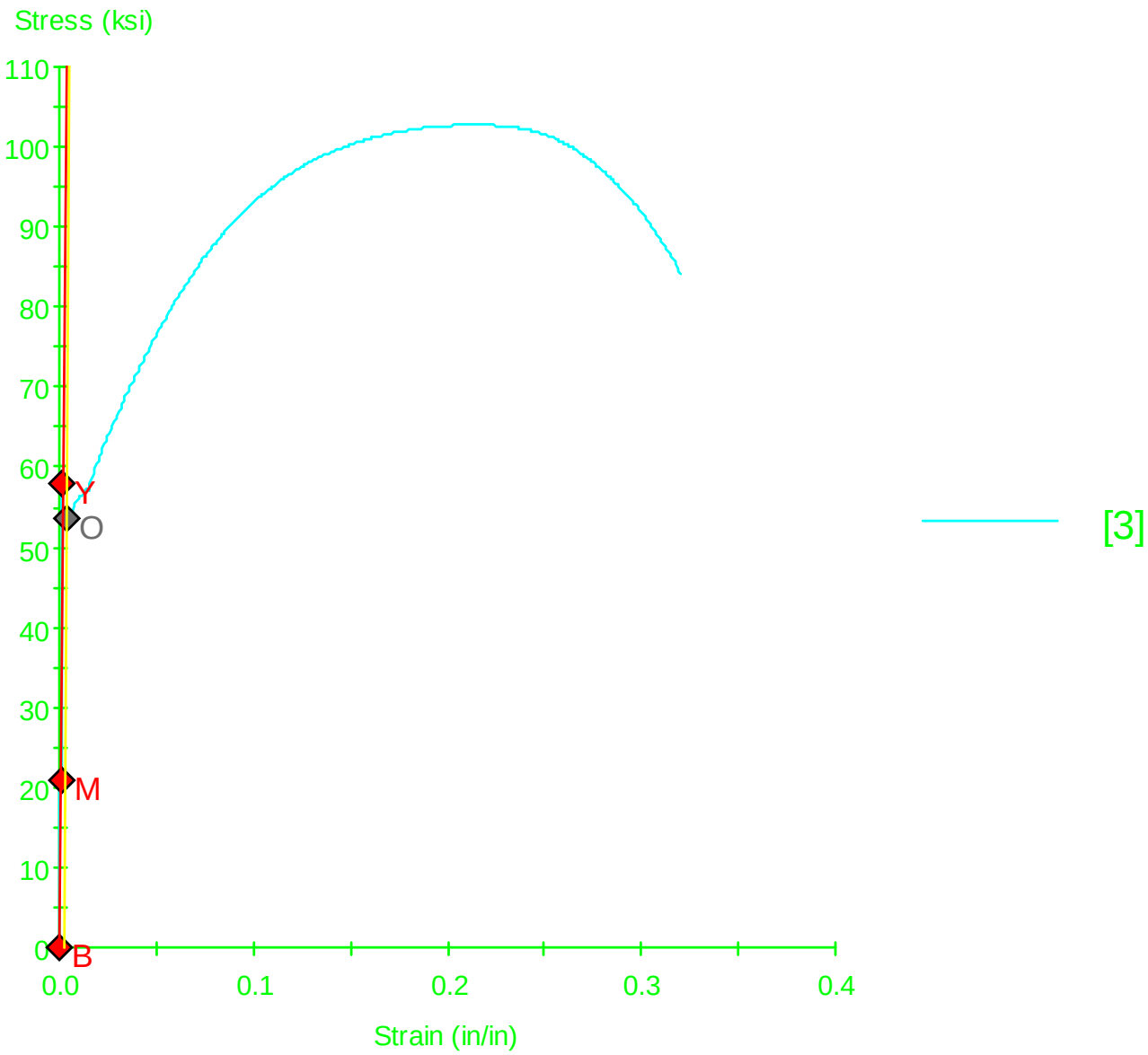
Stress (ksi)
110
100
90
80
70
60
50
40
30
20
10
0
Y
O
M
B
0.0
0.1
0.2
0.3
0.4
Strain (in/in)
[3]

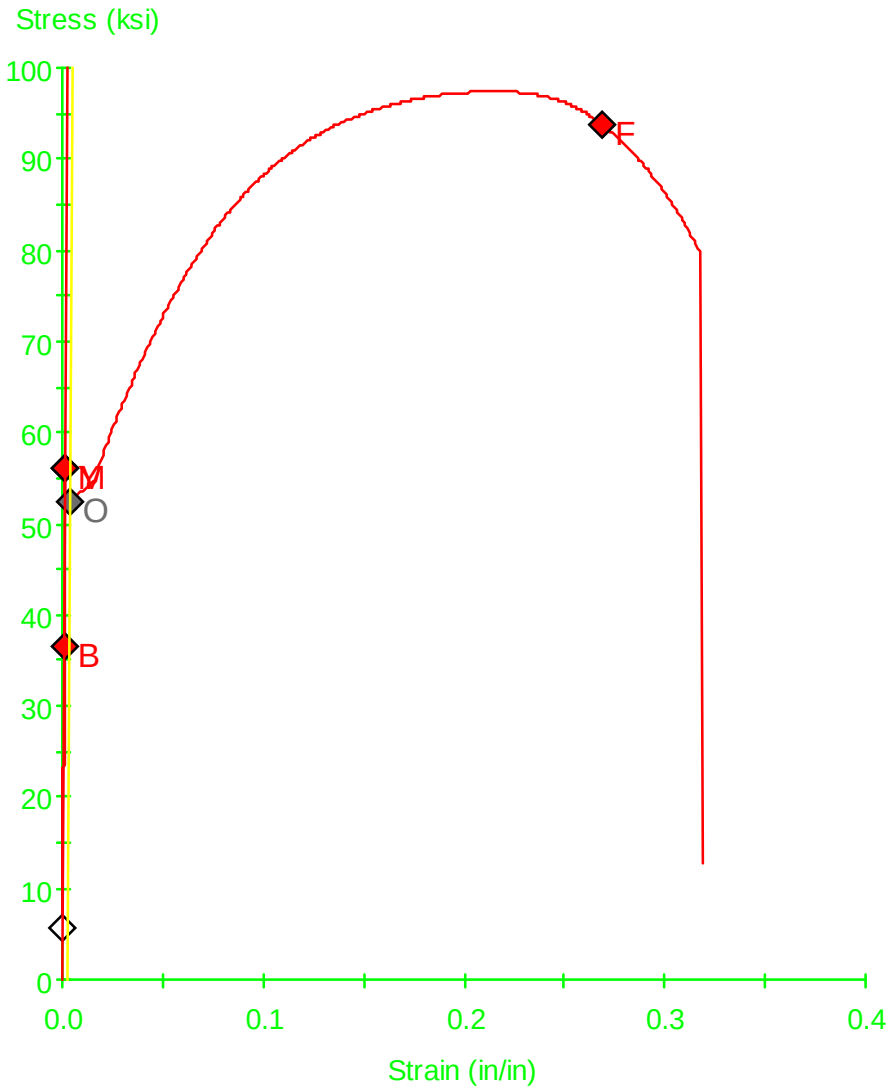
Stress (ksi)
100
90
80
70
60
50
40
30
20
10
0
F
M
O
B
0.0
0.1
0.2
0.3
0.4
Strain (in/in)

[4]

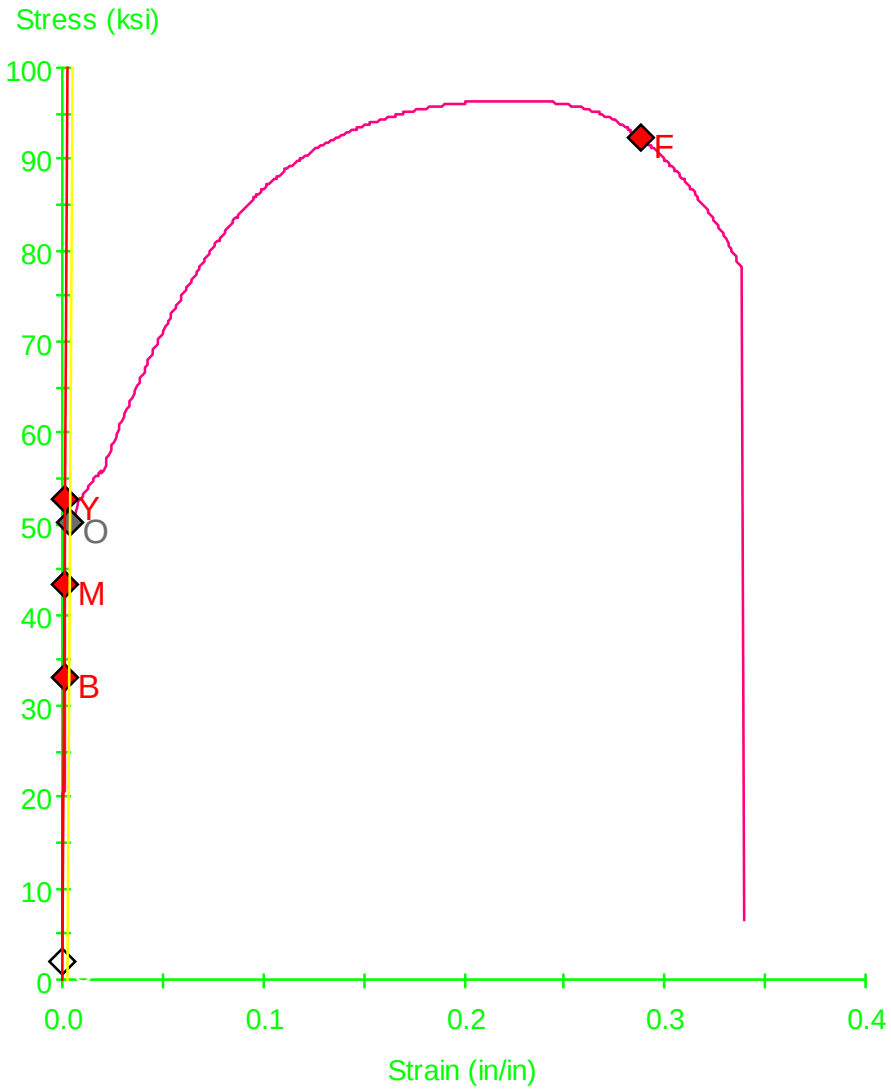
Stress (ksi)
100
90
80
70
60
50
40
30
20
10
0
Y
O
M
B
F
0.0
0.1
0.2
0.3
0.4
Strain (in/in)

[5]

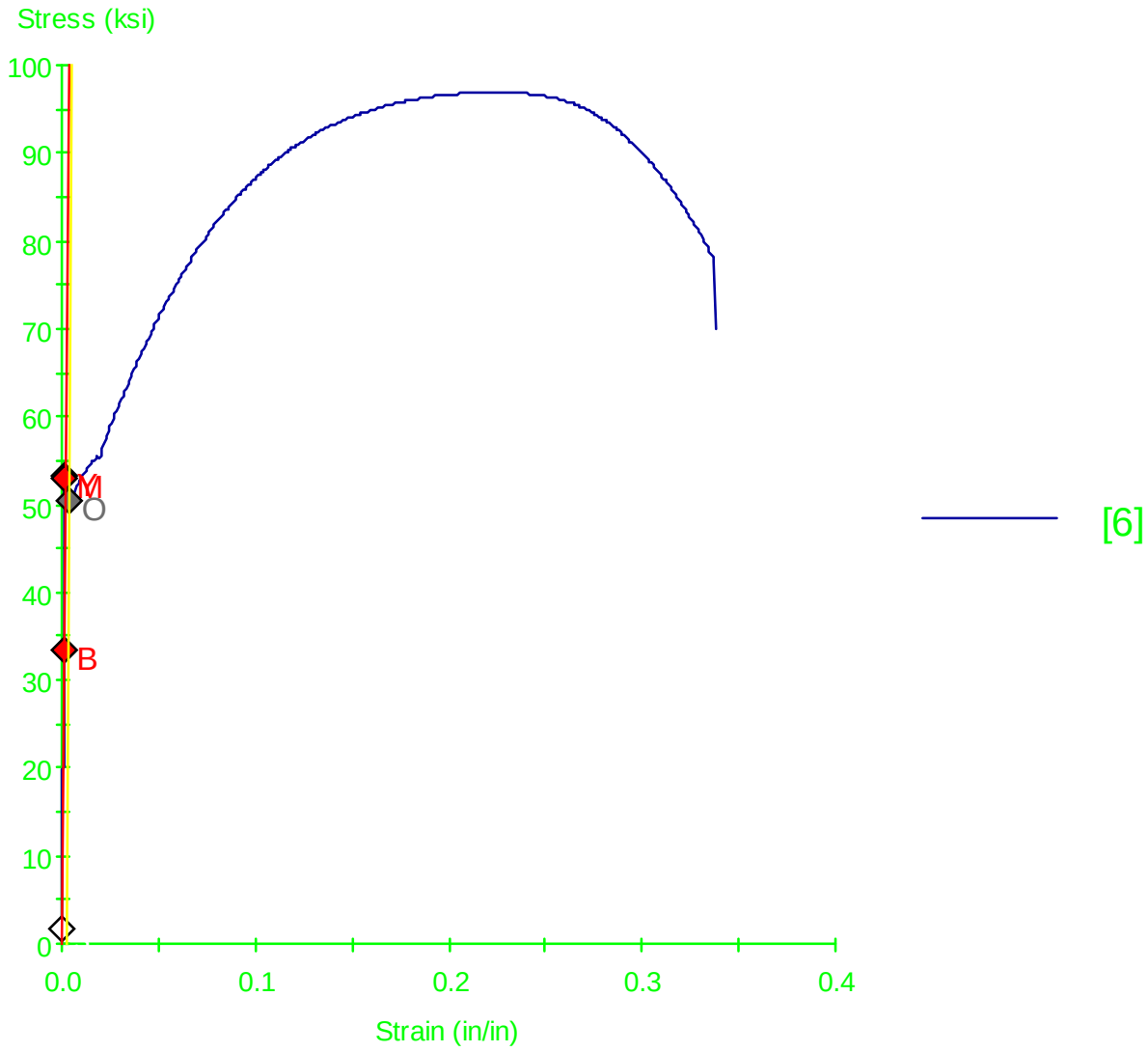
Stress (ksi)
100
90
80
70
60
50
40
30
20
10
0
M
O
B
0.0
0.1
0.2
0.3
0.4
Strain (in/in)
[6]